JOURNAL OF SOLID STATE CHEMISTRY 4, 29–37 (1972)

Crystal Structure and Mössbauer Effect Investigation of $FeVO_4$

B. ROBERTSON

Division of Natural Sciences and Mathematics, University of Saskatchewan, Regina, Saskatchewan, Canada

AND

E. KOSTINER

Baker Laboratory of Chemistry, Cornell University, Ithaca, New York 14850

Received March 25, 1971

The crystal structure of $FeVO_4$ has been determined. The space group is triclinic, $P\bar{1}$, with $a = 6.719(7)$, $b = 8.060(9)$, $c = 9.254(9)$ Å, $\alpha = 96.65(8)$, $\beta = 106.57(8)$, $\gamma = 101.60(8)°$ with $Z = 6$. Three independent iron atoms (two in distorted octahedral and one in a distorted trigonal bipyramidal environment) are joined to create a doubly bent chain of six edge-sharing polyhedra. The chains are joined by VO_4^{3-} tetrahedra. High resolution Mössbauer effect spectroscopy identifies the iron ions as trivalent and an assignment is made on the basis of the structure analysis. The structure is discussed in terms of Baur's correlation of bond length and bond environment.

Introduction

The compound $FeVO_4$ is one of the few binary transition metal oxides whose crystal structure has not been previously determined. Its occurrence as an incongruently melting compound in the Fe_2O_3–V_2O_5 system has been reported (*1*) along with the fact that it transforms under high pressure to an orthorhombic disordered-wolframite structure type (*2, 3*). During the course of this investigation, a note reporting the crystal growth and magnetic behavior of $FeVO_4$ appeared (*4*) indicating antiferromagnetic ordering with a Néel temperature of 22 ± 1°K. The published room temperature Mössbauer effect data (*4*) indicates at least two nonequivalent trivalent iron ions with a broad resonance spectrum at 4.2°K. Preliminary published single crystal X-ray diffraction data (*4*) indicate a triclinic unit cell with lattice parameters in good agreement with our results.

This paper reports the complete three-dimensional crystal structure determination and an analysis of the Mössbauer effect data for $FeVO_4$.

Experimental

Crystal Growth. Sound single crystals of $FeVO_4$ were grown by a standard melt technique. A mixture of reagent grade Fe_2O_3 and V_2O_5 in a mole ratio of one to two was placed in a tightly covered platinum crucible and heated to 975°C in a resistance heated furnace. Dry oxygen was passed through the furnace to prevent reduction of the transition metal ions. After soaking at this temperature for six hours the furnace was cooled to 650°C at 8°C/hr, the crucible removed from the furnace and allowed to cool to room temperature. Repeated washing with hot dilute nitric acid effectively removed the excess V_2O_5. Rod-shaped crystals up to 1 cm long and 1.5 mm in cross section were easily separated from the mixture. Chemical analysis confirmed the composition as $FeVO_4$.

Mössbauer Data. The ^{57}Fe Mössbauer effect was measured with a Model NS-1 Mössbauer spectrometer (Nuclear Science and Engineering Corp., Pittsburgh, Pa.) operating in the constant-acceleration mode. The 14.4-keV γ radiation from a source of ^{57}Co (15 mCi) diffused into palladium was detected with a gas proportional counter and collected with a 400-channel analyzer operating in time sequence scaling mode. The source and drive were calibrated against a single crystal of sodium nitroprusside (National Bureau of Standards, Standard Reference Material No. 725). The quadrupole splitting for sodium nitroprusside was taken as

1.7048 ± 0.0025 mm/sec. (*5*). Isomer shifts are reported with respect to the zero position of this standard. Sample thickness was 25 mg/cm^2 (corresponding to 8.2 mg of Fe/cm^2). The data were reduced by a computer program which performed a nonlinear least-squares fit to the product of a series of resonant absorption peaks having Lorentzian shapes superposed on a parabolic base line, a result of our particular drive geometry. All of the variables (peak position, peak height, and peak half-width) were allowed to vary independently.

X-ray Diffraction Data. The crystals showed no symmetry or extinctions in their diffraction patterns. Three arbitrary axes were chosen and the program DELRED written by L. T. Tai (*6*) was used to find the reduced cell using the Delaunay method.

A number of crystals with dimensions between 0.5 and 1 mm were selected and were circulated vigorously in a Nonius Crystal Grinder for approximately 24hr using a carborundum grinding surface. Although this was not a sufficient grinding time to obtain spherical crystals, a suitable crystal was selected with radius $0.17 \pm .02$ mm. The orientations of 29 reflections with 2θ values extending up to 55° were collected on a Picker four-circle diffractometer. The cell constants and orientation parameters were determined in a PICK II least-squares refinement program; cell constants obtained in this way were $a = 6.719(7)$, $b = 8.060(9)$, $c = 9.254(9)$Å, $\alpha = 96.65(8)$, $\beta = 106.57(8)$, $\gamma = 101.60(8)°$. The numbers in parentheses represent meaningful standard deviations in the last reported figure.

Integrated intensities of 3174 independent reflections were collected on the diffractometer using a highly oriented graphite monochromator and a continuous scan rate of one degree per minute in the θ–2θ mode with Mo$K\alpha$ radiation and a take-off angle of 3.0°. The 2θ base width was set at 2.1° and the background on either side of each peak was counted for 10 sec. The data extended to 64° in 2θ which corresponds to a volume of reciprocal space approximately one and one half times that available in the copper sphere. Three standard reflections were measured after each set of approximately 200 data points had been collected. These were plotted against time and showed no significant systematic trends.

The data were reduced to observed structure factors $|F_0|$ by the usual procedures. The Lorentz and polarization correction factor used in this work was

$$(\cos^2 2\theta_m + \cos^2 2\theta_s)/2 \sin 2\theta_s,$$

where θ_m and θ_s are the Bragg angles for the monochromator and sample, respectively. The estimated standard deviation based on counting statistics for each $|F_0|$ was supplemented by the factor $0.50 + 0.005\,|F_0|$ as an *ad hoc* attempt to allow for systematic errors in determining the standard deviation σ. Reflections whose intensities appeared negative were set to zero and reflections for which $|F_0| < 2\sigma$ were labelled as weak reflections.

The number of remaining reliable reflections was 2932. Only these reflections were used for the solution of the structure and the initial least-squares refinement, but all reflections were retained and used for the final cycles of refinement. The Mössbauer spectrum (*vide infra*) at this point suggested the number of formula units per unit cell to be a multiple of three. Six formula units give a calculated density of 3.65 compared to a measured density (buoyant force) of 3.63(1). The linear absorption coefficient for Mo$K\alpha$ radiation is 80 cm^{-1} with six formula units in the unit cell. Absorption corrections were made by interpolating the correction curves for a spherical crystal (*7*). An overall temperature factor, scale constant, and individual normalized structure factors were calculated using Wilson statistics. Scattering factors were determined from the series coefficients calculated by Cromer and Mann (*8*) for ionization states Fe^{+3}, V^{+2} and O^-. The average values of $|E^2 - 1|$ and $|E|$ were 1.009 and 0.797, in good agreement with the predicted values of 0.968 and 0.798 for a centrosymmetric structure. The space group was thus assumed to be $P\bar{1}$.

Determination of the Structure

A Patterson map was calculated using approximately 600 low angle reflections. A three-atom solution which fit the six largest peaks of the Patterson map gave an agreement factor of 0.48, and was used to assign phases of the low angle reflections in an electron density Fourier calculation. The expression for the agreement factor used in this work is

$$R_\omega = \left(\frac{\Sigma\omega||F_0| - |F_c||^2}{\Sigma\omega|F_0|^2}\right)^{1/2}, \qquad \text{where } \omega = \frac{1}{\sigma^2}.$$

Atoms were assigned to all the significant peaks in the new map and individual atoms were subsequently rejected if either the least-squared multiplicity of the atom was low or its geometry with respect to the starting atoms was chemically unacceptable. Atoms which survived this elimination procedure were then used to determine the next set of phases. This was repeated several times to find all the atoms in the structure except in the final stages where difference Fourier maps were also used. When the R factor

had been lowered to 0.20, the restrictions of centrosymmetry were dropped to accommodate a number of atoms with multiplicities near one-half. The structure solution was then completed using the space group $P1$. However, large off-diagonal terms in the variance–covariance matrix of the least-squares refinement indicated the presence of an alternative true center of symmetry, removed several angstroms from the local center corresponding to the partial solution to the Patterson function. The structure was refined by full-matrix least-squares using all the data and individual anisotropic temperature factors in the space group $P\bar{1}$ using a highly modified version of the program ORFLS (*9*). The imaginary part of the anomalous dispersion corrections (*10*) was applied to the scattering factors of iron and vanadium. Real parts of the anomalous dispersion are smaller and were ignored. The standard deviations used in the weighting scheme for the final cycles of least-squares was

$$\sigma = 1.09 - 0.040|F_0| + 0.0012|F_0|^2.$$

These coefficients were determined by fitting a curve to a plot of

$$\Delta = ||F_0| - |F_c||$$

plotted as a function of $|F_0|$. This procedure assumes that the errors in F_c arising from the inadequacies of the model used to calculate F_c are less than Δ and thus the average value of Δ within a small range of $|F_0|$ is assumed to be a good approximation to σ. The final R factors were 0.047 both for all the data taken collectively and for the reliable data alone.[1] The weak reflections were considered to be in complete agreement if $|F_c|$ was less than $|F_0|$.

Table I lists the final atomic coordinates and thermal parameters for each atom in $FeVO_4$. The magnitudes of the thermal parameters for a given species of atom depend in part on the choice of scattering factor curve for that atom, and in this case the best choice for the V^{5+} ions is not clear. However, the thermal parameters suggest that the mean square deviations of the Fe^{3+} and V^{5+} ions from their equilibrium positions are nearly isotropic

[1] A table of observed and calculated structure amplitudes from this analysis has been deposited as Document No. NAPS-01574 with the ASIS National Auxiliary Publication Service, c/o CCM Information Corp., 909 Third Avenue, New York, N.Y. 10022. A copy may be secured by citing the document number and by remitting $5 for photocopies or $2 for microfiche. Advance payment is required. Make check or money order payable to ASIS-NAPS.

TABLE I

FRACTIONAL COORDINATES AND THERMAL PARAMETERS FOR $FeVO_4$[a]

	x/a	y/b	z/c	U_{11}	U_{22}	U_{33}	U_{12}	U_{13}	U_{23}
Fe(1)	0.75204(17)	0.69423(14)	0.40881(12)	5.4(5)	4.9(4)	5.8(4)	0.6(4)	2.2(4)	0.5(3)
Fe(2)	0.46597(17)	0.88944(14)	0.21160(12)	4.7(4)	5.7(4)	6.9(4)	0.6(3)	2.3(3)	1.6(4)
Fe(3)	0.96885(17)	0.30568(14)	0.01195(12)	5.0(4)	4.6(4)	5.6(4)	0.3(3)	1.8(3)	−0.4(3)
V(1)	0.00496(19)	0.99694(16)	0.25674(14)	4.1(5)	3.8(5)	4.6(5)	0.4(4)	2.7(4)	0.1(4)
V(2)	0.19955(19)	0.60155(16)	0.34332(14)	4.0(5)	5.1(5)	4.5(5)	0.1(4)	2.3(4)	0.4(4)
V(3)	0.52063(19)	0.29906(16)	0.12734(14)	4.3(5)	3.8(5)	6.4(5)	0.1(4)	2.9(4)	−1.0(4)
O(1)	0.6451(10)	0.4844(8)	0.2514(7)	15(3)	8(2)	13(3)	−2(2)	4(2)	−3(2)
O(2)	0.2548(10)	0.4375(8)	0.4260(7)	14(3)	11(3)	11(3)	3(2)	4(2)	4(2)
O(3)	0.0526(10)	0.6990(8)	0.4280(7)	8(2)	14(3)	12(3)	2(2)	6(2)	−3(2)
O(4)	0.1586(10)	0.0954(8)	0.4291(7)	12(3)	9(2)	9(2)	0(2)	3(2)	−2(2)
O(5)	0.4530(9)	0.7388(8)	0.3611(7)	6(2)	11(2)	10(2)	1(2)	4(2)	5(2)
O(6)	0.7611(9)	0.8670(7)	0.2649(7)	5(2)	9(2)	9(2)	0(2)	2(2)	4(2)
O(7)	0.5273(11)	0.1277(8)	0.2197(8)	17(3)	7(2)	20(2)	3(2)	8(2)	5(2)
O(8)	0.1514(9)	0.8720(8)	0.1772(7)	7(2)	10(2)	10(2)	2(2)	4(2)	−3(2)
O(9)	0.3569(9)	0.7308(8)	0.0193(7)	7(2)	12(2)	9(2)	1(2)	3(2)	−1(2)
O(10)	0.2641(10)	0.2960(9)	0.0385(7)	6(2)	22(3)	14(3)	5(2)	3(2)	1(2)
O(11)	0.9495(10)	0.1452(4)	0.1524(8)	13(3)	15(3)	17(3)	5(2)	7(2)	9(2)
O(12)	0.0537(9)	0.5273(7)	0.1472(6)	10(2)	8(2)	6(2)	0(2)	2(2)	0(2)

[a] The parameters U_{ij} are calculated from $U_{ij} = \beta_{ij}/(2\pi^2 b_i b_j)$ where the b_i are the reciprocal axial lengths and the β_{ij} appear as a temperature effect through $\exp(-\beta_{11}h^2 + \cdots + 2\beta_{12}hk + \cdots)$. The values are given as U_{ij} multiplied by 10^3 and have units $Å^2$. The numbers in parentheses are estimated standard deviations from the least-squares analysis, multiplied by three.

and small in comparison with those of the oxygen atoms.

Discussion of the Structure

The pertinent interatomic distances and angles are listed in Table II. Two of the three independent iron atoms are in distorted octahedral environments of six oxygen atoms. The third iron atom is in a distorted trigonal bipyramidal environment of five oxygen atoms. Angles subtended at the iron atoms by the oxygen atoms deviate from the idealized values by up to 16°. The bond lengths [Fe^{3+}–O^{2-}] range from 1.869 to 2.114 Å. The three independent vanadium atoms are each in slightly distorted tetrahedral environments of oxygen atoms. The angles

TABLE II

STRUCTURAL GEOMETRY OF $FeVO_4$[a]

(*a*) Fe–O_n groups

(*i*) Interatomic distances (Å)

$\sigma[Fe^{3+}–O^{2-}] = 0.006$

$\sigma[O^{2-}–O^{2-}] = 0.009$

$\sigma[Fe^{3+}–Fe^{3+}] = 0.002$

	[Fe^{3+}–O^{2-}]	O Coord. No.	P_O	$(1.56 + 0.22\,P_O)$
Fe(1)–O(1)	1.969	2	1.75	1.95
–O(2)	1.980	2	1.75	1.95
–O(3)	1.968	2	1.75	1.95
–O(4)	2.003	2	1.75	1.95
–O(5)	2.045	3	2.35	2.08
–O(6)	2.049	3	2.35	2.08
Average 2.002				
Fe(2)–O(5)	1.964	3	2.35	
–O(6)	1.953	3	2.35	
–O(7)	1.869	2	1.85	
–O(8)	2.018	3	2.35	
–O(9)	1.936	3	2.35	
Average 1.948				
Fe(2)–O(8)	1.992	3	2.35	2.08
–O(9)	2.078	3	2.35	2.08
–O(10)	1.946	2	1.75	1.95
–O(11)	1.959	2	1.75	1.95
–O(12)	1.942	3	2.25	2.06
–O(12′)	2.114	3	2.25	2.06
Average 2.005				

Fe(1) Octahedron		Fe(2) Trigonal bipyramid		Fe(3) Octahedron	
O(1)–O(2)	2.861	O(5)–O(6)	2.565	O(8)–O(9)	2.606
O(1)–O(3)	2.841	O(5)–O(7)	3.540	O(8)–O(10)	2.886
O(1)–O(5)	2.874	O(5)–O(8)	2.745	O(8)–O(11)	2.942
O(1)–O(6)	3.003	O(5)–O(9)	3.066	O(8)–O(12′)	2.685
O(2)–O(3)	2.895	O(6)–O(7)	2.867	O(9)–O(11)	2.670
O(2)–O(4)	2.708	O(6)–O(8)	2.957	O(9)–O(12)	2.975
O(2)–O(5)	3.064	O(6)–O(9)	2.919	O(9)–O(12′)	2.962
O(3)–O(4)	2.839	O(7)–O(8)	2.816	O(10)–O(11)	2.762
O(3)–O(6)	2.800	O(7)–O(9)	3.313	O(10)–O(12)	2.819
O(4)–O(5)	2.742	O(8)–O(9)	2.606	O(10)–O(12′)	3.047
O(4)–O(6)	2.726			O(11)–O(12)	3.027
O(5)–O(6)	2.565			O(12)–O(12′)	2.600
		Fe(1)–Fe(2)	3.073		
		Fe(2)–Fe(3)	3.048		
		Fe(3)–Fe(3′)	3.119		

TABLE II—*continued*

(*ii*) Angles (deg)

Fe(1) Octahedron		Fe(2) Trigonal bipyramid		Fe(3) Octahedron	
O(1)–Fe(1)–O(2)	92.9	O(5)–Fe(2)–O(7)	134.9	O(8)–Fe(3)–O(9)	79.6
O(1)–Fe(1)–O(3)	92.4	O(5)–Fe(2)–O(9)	103.7	O(8)–Fe(3)–O(10)	94.3
O(1)–Fe(1)–O(5)	91.4	O(7)–Fe(2)–O(9)	121.1	O(8)–Fe(3)–O(4)	96.3
O(1)–Fe(1)–O(6)	96.7	O(6)–Fe(2)–O(5)	81.8	O(8)–Fe(3)–O(12′)	81.6
O(2)–Fe(1)–O(3)	94.4	O(6)–Fe(2)–O(7)	97.1	O(9)–Fe(3)–O(11)	82.8
O(2)–Fe(1)–O(4)	85.7	O(6)–Fe(2)–O(9)	97.3	O(9)–Fe(3)–O(12)	95.4
O(2)–Fe(1)–O(5)	99.2	O(8)–Fe(2)–O(5)	87.1	O(9)–Fe(3)–O(12′)	89.9
O(3)–Fe(1)–O(4)	91.3	O(8)–Fe(2)–O(7)	92.8	O(10)–Fe(3)–O(11)	90.0
O(3)–Fe(1)–O(6)	88.3	O(8)–Fe(2)–O(9)	82.4	O(10)–Fe(3)–O(12)	92.9
O(4)–Fe(1)–O(5)	85.3	O(6)–Fe(2)–O(8)	168.5	O(10)–Fe(3)–O(12′)	92.4
O(4)–Fe(1)–O(6)	84.5			O(11)–Fe(3)–O(12)	101.8
O(5)–Fe(1)–O(6)	77.6			O(12)–Fe(3)–O(12′)	79.6
O(1)–Fe(1)–O(4)	176.1			O(8)–Fe(3)–O(12)	160.6
O(2)–Fe(1)–O(6)	169.9			O(11)–Fe(3)–O(12′)	172.6
O(3)–Fe(1)–O(5)	165.7			O(9)–Fe(3)–O(10)	169.9

(*b*) VO_4 groups

(*i*) Interatomic distances (Å)

$\sigma[V^{5+}–O^{2-}] = 0.007$

$\sigma[O^{2-}–O^{2-}] = 0.009$

	$[V^{5+}–O^{2-}]$	O Coord. No.	P_o	$(1.43 + 0.15\,P_o)$
V(1)–O(4)	1.649	2	1.75	1.66
–O(6)	1.785	3	2.35	1.78
–O(8)	1.783	3	2.35	1.78
–O(11)	1.662	2	1.75	1.66
V(2)–O(2)	1.660	2	1.75	1.66
–O(3)	1.683	2	1.75	1.66
–O(5)	1.786	3	2.35	1.78
–O(12)	1.780	3	2.25	1.77
V(3)–O(1)	1.679	2	1.75	1.66
–O(7)	1.713	2	1.85	1.71
–O(9)	1.806	3	2.35	1.78
–O(10)	1.680	2	1.75	1.66

(*ii*) Angles (deg)

V(1) Tetrahedron		V(2) Tetrahedron		V(3) Tetrahedron	
O(4)–V(1)–O(6)	109.9	O(2)–V(2)–O(3)	109.4	O(1)–V(3)–O(7)	108.2
O(4)–V(1)–O(8)	108.0	O(2)–V(2)–O(5)	105.6	O(1)–V(3)–O(9)	112.2
O(4)–V(1)–O(11)	108.6	O(2)–V(2)–O(12)	110.3	O(1)–V(3)–O(10)	110.9
O(6)–V(1)–O(8)	111.9	O(3)–V(2)–O(5)	113.2	O(7)–V(3)–O(9)	108.2
O(6)–V(1)–O(11)	109.2	O(3)–V(2)–O(12)	109.4	O(7)–V(3)–O(10)	108.9
O(8)–V(1)–O(11)	109.1	O(5)–V(2)–O(12)	108.9	O(9)–V(3)–O(10)	106.4

(*c*) Angles subtended at three-coordinated oxygen atoms (deg)

Fe(1)–O(5)–Fe(2)	100.0	Fe(1)–O(6)–Fe(2)	100.2	Fe(2)–O(8)–Fe(3)	98.9
Fe(1)–O(5)–V(2)	131.3	Fe(1)–O(6)–V(1)	123.1	Fe(2)–O(8)–V(1)	134.2
Fe(2)–O(5)–V(2)	118.1	Fe(2)–O(6)–V(1)	133.7	Fe(3)–O(8)–V(1)	125.8
Sum	349.4	Sum	357.0	Sum	358.9
Fe(2)–O(9)–Fe(3)	98.7	Fe(3)–O(12)–Fe(3′)	100.4		
Fe(2)–O(9)–V(3)	129.6	Fe(3)–O(12)–V(2)	134.2		
Fe(3)–O(9)–V(3)	126.4	Fe(3′)–O(12)–V(2)	122.3		
Sum	354.7	Sum	356.9		

[a] Corrections for thermal motion were found not to significantly alter the bond lengths and, therefore, none were applied. Estimated standard deviations are reported. P_o is the "sum of electrostatic bond strengths" as defined by Pauling (*14*) for the corresponding oxygen atoms. Where appropriate, predicted bond lengths are given based on P_o (see text).

subtended at the vanadium atoms by the oxygen atoms vary from the ideal value of 109.5° by an average of 1.4° with a maximum deviation of 3.9°. However, the bond lengths [V^{5+}–O^{2-}] range from 1.660 Å to 1.806 Å, depending on the environment of the oxygen atom.

The three independent iron atoms and those related by the center of symmetry at ($\frac{1}{2}$00) join to create a doubly-bent chain of six edge-sharing polyhedra formed by the oxygen atoms coordinated to the six iron atoms. Figure 1 shows this chain projected onto the *a–b* plane. The chains are joined by VO_4 tetrahedra. Figure 2 shows all the doubly-bent chains joined to one such chain through the tetrahedra, as projected onto the *b–c* plane. The iron–iron interatomic distances within the chain (also listed in Table II) show the largest separation between the two octahedrally coordinated iron atoms at the center of the chain; but the total variation in the [Fe^{3+}–Fe^{3+}] distances is small. The principal distortion of the polyhedra is that resulting from the ionic repulsion between the iron atoms in two adjacent polyhedra. The angle subtended at the iron atoms by each pair of oxygen atoms forming a shared edge is less than the value expected for the regular polyhedra (which is 90° in each case) by 7.6–12.4°, and the length of these edges is shorter than other unshared edges of the same polyhedron by an average distance of 0.26 Å, a magnitude which is similar to the approximate value of the shortening of shared edges as discussed elsewhere (*11*). The VO_4 tetrahedra share corners with up to four polyhedra within a single chain, but none of them share an edge with an individual polyhedron in a chain.

Direct cation–cation magnetic exchange interactions and cation–anion–cation superexchange interactions between adjacent iron atoms with the d^5 configuration give antiferromagnetic coupling (*12*). The cation–anion–cation superexchange energy term allows antiferromagnetic coupling over the full range of Fe–O–Fe angles from 90° to 180° with the maximum energy expected at 180°. The dominant factor in creating the relative complexity of the structure seems to be the sharing of polyhedral edges, as a result of which the Fe–O–Fe angles are limited to approximately 100° and would indicate little superexchange interaction. The antiferromagnetic coupling must be the result of direct exchange as are the local charge imbalances derived from the marked differentiation of the structure into areas containing V^{5+} ions and areas containing Fe^{3+} ions.

On the average, the bonds to the five-coordinated

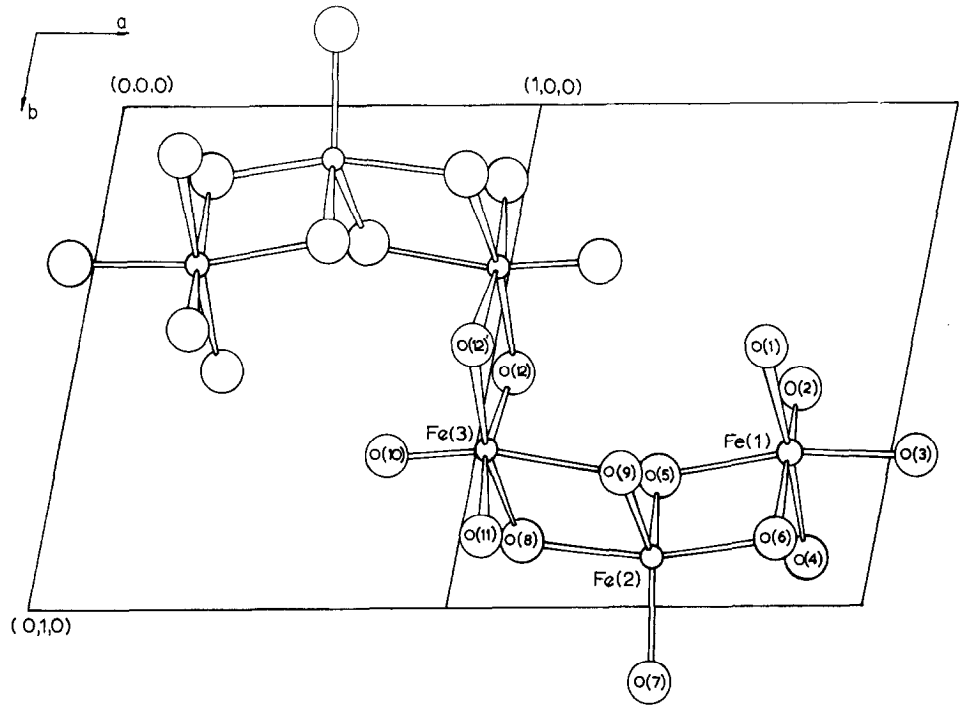

FIG. 1. The doubly bent chain of six iron atoms in $FeVO_4$ projected onto the *a–b* plane. The large circles are oxygen atoms and the small are iron atoms.

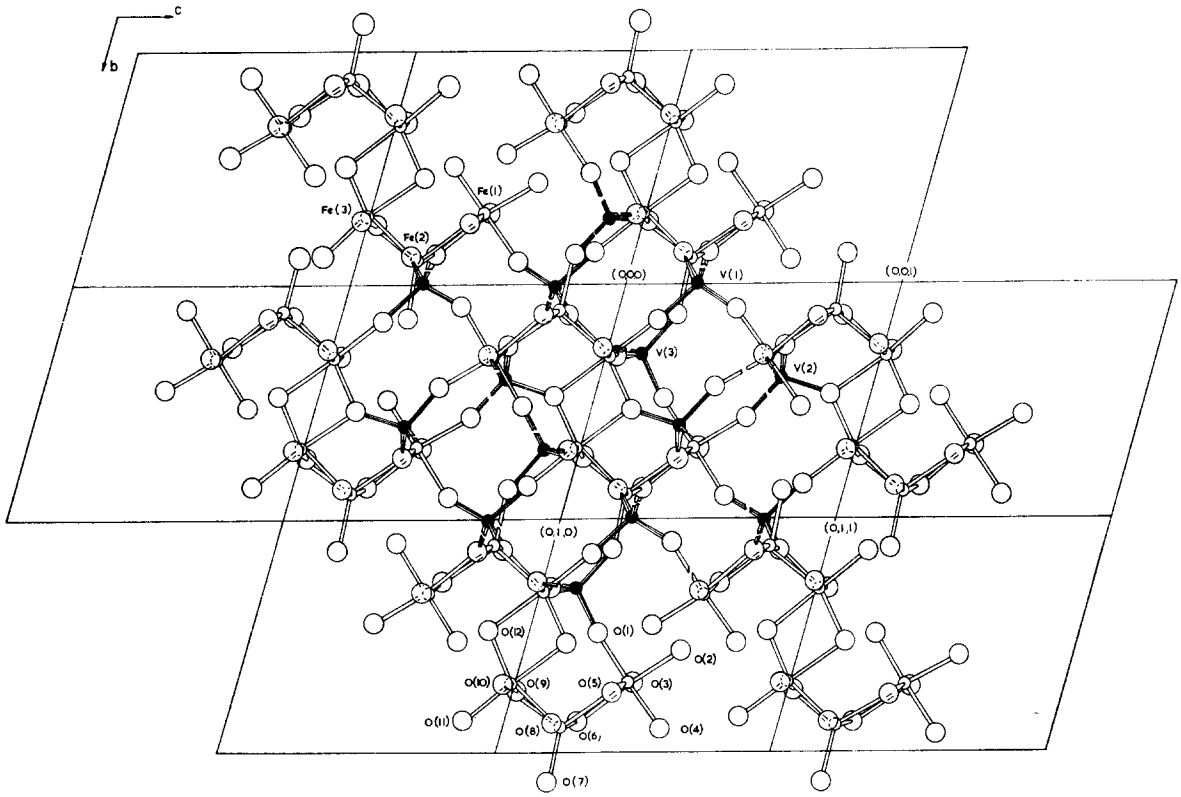

FIG. 2. The structure of $FeVO_4$ projected onto the *b*–*c* plane, showing all the chains of six iron atoms joined to one central chain through VO_4 tetrahedra. The large open circles are oxygen atoms, the small open circles are iron atoms and the small filled circles are vanadium atoms.

iron atoms are shorter than those to the six-coordinated iron atoms. Furthermore, there is a tendency for bonds to two-coordinated oxygen atoms to be shorter than those to three-coordinated oxygen atoms although significant exceptions are evident. Baur (*13*) has suggested a phenomenological method of correlating bond lengths and bond environment. For a particular cation A in a coordination polyhedron of one species of anions X, the bond lengths are predicted from $[A - X] = (a + bP_X)A$, where a and b are empirical constants obtained from existing structural data, and P_X is the "sum of the electrostatic bond strengths" parameter introduced by Pauling (*14*), where

$$P_X = \sum_i \frac{Z_i}{C.N._i},$$

Z_i is the formal charge on the ith cation bonded to X, and $C.N._i$ is the coordination number of that cation. For FeO_6 polyhedra Baur has proposed the expression $[Fe^{3+}\text{–}O^{2-}] = 1.56 + 0.22P_O$. Bond lengths calculated with these constants and P_O are listed in Table II(a) for the octahedrally coordinated iron atoms. Krishnamachari and Calvo (*15*) have proposed the expression $[V^{5+}\text{–}O^{2-}] = 1.43 + 0.15P_O$ for VO_4 tetrahedra. Bond lengths calculated with these constants and P_O are listed in Table II(b) and compare favorably with the observed values. The average discrepancies between observed and calculated bond lengths for $[V^{5+}\text{–}O^{2-}]$ and $[Fe^{3+}\text{–}O^{2-}]$ are 0.01 Å and 0.04 Å, respectively. These comparisons suggest that if the method given by Baur for predicting bond lengths is valid, the structural geometry of the doubly bent chain imposes limitations on the $[Fe^{3+}\text{–}O^{2-}]$ interatomic distances which do not allow optimum $Fe^{3+}\text{–}O^{2-}$ bonding.

Although most mixed metal oxides may be discussed in relation to close packed layers of oxygen atoms, no additional rationalization of this structure is obtained by attempting to describe it as a distorted derivative of any such close packed layer structure. The mechanism for a transformation to a wolframite-type structure for $FeVO_4$ prepared at 750°C and 60 000 atm (*2*, *3*) is not readily seen from the crystal

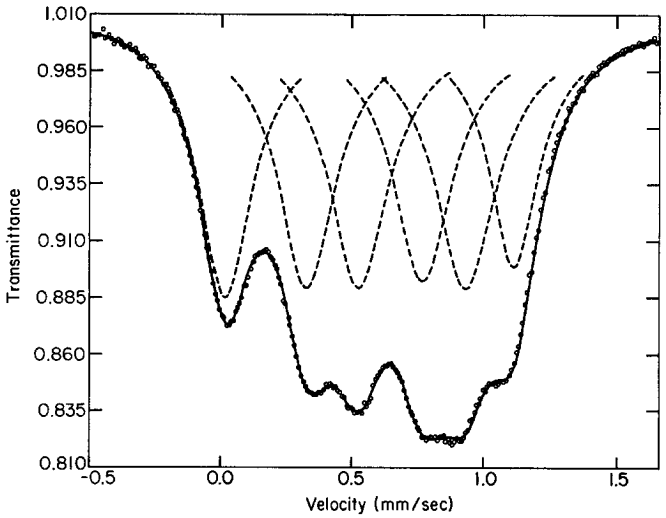

FIG. 3. Mössbauer spectrum of $FeVO_4$ at room temperature. Velocity scale is relative to sodium nitroprusside. Solid line is the least-squares fit, dashed lines are the individual peaks and circles indicate the normalized data. See text for peak assignment.

structure determined in this work. However, the increase in the coordination numbers of five and six for the iron and four for the vanadium atoms to six for all of the metal atoms in the high-pressure form results in a large increase in the calculated densities—from 3.65 to 4.72 g/cc, a 29.3% increase. Certainly this reflects not only this increase in coordination number but also the compression of the rather open chain structure of the low pressure form to the approximately hexagonal close-packed array of oxygen atoms of the high pressure form.

Discussion of the Mössbauer Data

The room temperature Mössbauer effect spectrum (Fig. 3) exhibits six resonance lines of essentially equal area. Table III lists each of these six lines (numbering from left to right), its position relative to the sodium nitroprusside standard, relative area and full width at half maximum (FWHM).

Since each of the three iron atoms lies in a distorted polyhedron of oxygen atoms, it is reasonable to assume that these six lines represent a set of three resonance absorptions, each a quadrupole-split doublet. The assignment of these resonance pairs is made as follows. Five-coordinated Fe^{+3} should exhibit a large quadrupole splitting; in fact, Fe^{+3} substituted for Mn^{+3} in the hexagonal phase $YMnO_3$ (trigonal pyramidal coordination about the manganese ion) shows a quadrupole splitting of 2.03 mm/sec (*16*), a large value for high-spin Fe^{+3}. Of the possible combinations of the six resonance lines, the pair 1–6 gives a quadrupole splitting of 1.113 mm/sec and a resulting isomer shift of +0.582 mm/sec; this pair is assigned to Fe(2), the five-coordinated ion.

Literature values (*17*) for six-coordinate Fe^{+3} in oxidic materials show a range of isomer shifts of

TABLE III

ROOM TEMPERATURE MÖSSBAUER RESONANCE LINES

Line	Position[a]	Relative area	FWHM
1	0.025 mm/sec	1.00	0.26 mm/sec
2	0.340	1.00	0.26
3	0.540	1.06	0.28
4	0.787	1.02	0.28
5	0.953	1.09	0.29
6	1.138	0.81	0.24

[a] Estimated standard deviation: 0.004 mm/sec.

TABLE IV

ROOM TEMPERATURE MÖSSBAUER PARAMETERS

Lines	Isomer Shift[a,b]	Quadrupole Splitting[a]	
3–4	+0.664 mm/sec	0.247 mm/sec	Fe(1), Fe(3)
2–5	0.647	0.613	
1–6	0.582	1.113	— Fe(2)

[a] Estimated standard deviation: 0.004 mm/sec.
[b] Relative to sodium nitroprusside.

+0.62 to +0.75 mm/sec (relative to sodium nitroprusside). The nearly identical average iron–oxygen distances in the two six-coordinated polyhedra—Fe(1) and Fe(3)—should give rise to nearly identical isomer shifts since the *s*-electron contribution to the bonding would be similar. Inspection of the six possible combinations of the remaining four resonance lines indicate that resonance pairs 3–4 and 2–5 have close values of isomer shift and should be assigned to the two unique six-coordination sites. It has been observed (*8*) that there is a meaningful decrease in Fe^{57} isomer shifts with a decrease in coordination number. This further supports the assignment of the $IS = +0.582$ mm/sec pair to the five-coordinated Fe(2). Table IV summarizes the room-temperature Mössbauer parameters on the basis of these assignments. These parameters are all characteristic of high-spin trivalent iron ions in distorted coordination polyhedra (*17*).

At 4.2°K, below the antiferromagnetic ordering temperature, a broad magnetically split hyperfine spectrum is observed. As there should be a total of eighteen lines in this spectrum it is not surprising that it is not readily resolvable. Its character is in general agreement with that previously reported (*4*) with an overall magnetic hyperfine splitting of 465(15) *k*0*e*.

Acknowledgments

The authors wish to thank Mr. J. Marley for help with the data processing. This work was supported in part by a grant from the National Research Council of Canada (to B.R.) and in part by the Advanced Research Projects Agency through the Materials Science Center, Cornell University (to E.K.).

References

1. A. BURDESE, *Ann. Chim. Rome* **47**, 797 (1957).
2. A. P. YOUNG AND C. M. SCHWARTZ, *Acta Crystallogr.* **15**, 1305 (1962).
3. F. LAVES, A. P. YOUNG, AND C. M. SCHWARTZ, *Acta Crystallogr.* **17**, 1476 (1964).
4. L. M. LEVINSON AND B. M. WANKLYN, *J. Solid State Chem.* **3**, 131 (1971).
5. R. W. GRANT, R. M. HOUSLEY, AND U. GONSER, *Phys. Rev.* **178**, 523 (1969).
6. L. T. TAI AND R. E. HUGHES, "A Systematic Reformulation of the Delaunay Lattice Transformation", Report No. 1345, Materials Science Center, Cornell University, Ithaca, N.Y., 1970.
7. "International Tables for X-ray Crystallography: II. Mathematical Tables", The Kynoch Press, Birmingham. England, 1968.
8. D. T. CROMER AND J. B. MANN, *Acta Crystallogr. Sect. A* **24**, 321 (1968).
9. W. R. BUSING, K. O. MARTIN, AND H. A. LEVY, "ORFLS, A Fortran Crystallographic Least-Squares Program", ORNL-TM-305, Oak Ridge National Laboratory, Oak Ridge, Tenn., 1962.
10. D. T. CROMER, *Acta Crystallogr.* **18**, 17 (1965).
11. L. PAULING, "The Nature of the Chemical Bond", p. 559, Cornell University Press, Ithaca, N.Y., 1960.
12. J. B. GOODENOUGH, "Magnetism and the Chemical Bond," p. 165, John Wiley/Interscience, New York, 1963.
13. W. H. BAUR, *Trans. Amer. Crystallogr. Soc.* **6**, 129 (1970).
14. L. PAULING, *J. Amer. Chem. Soc.* **51**, 1010 (1929).
15. N. KRISHNAMACHARI AND C. CALVO, private communication.
16. J. CHAPPERT, *J. Phys.* **28**, 81 (1967).
17. J. DANON in "Chemical Applications of Mössbauer Spectroscopy" (V. I. Golldanskii and R. H. Herber, Eds.), Academic Press, New York, 1968.
18. N. N. ERICKSON in "The Mössbauer Effect and its Application in Chemistry" (R. F. Gould, Ed.), American Chemical Society, Washington, D.C., 1967.